Multiscale Electrothermal Simulation Techniques of GaN HEMTs

Yang Shen

Department of Engineering Mechanics, School of Aerospace Engineering,
Tsinghua University

April 25, 2022

GaN HEMTs

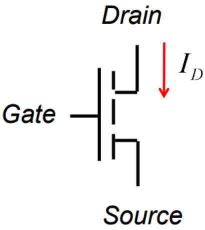

Figure 1: MOSFET circuit symbol.

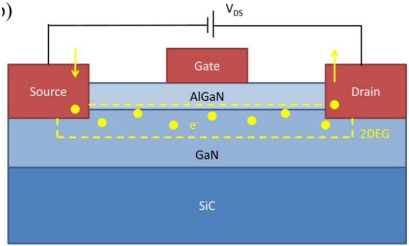

Figure 2: cross-section schematic of HEMT structure [1].

HEMT: High Electron Mobility Transistor.
The wide bandgap of the III-V material allows the HEMT to sustain a high voltage, the 2D electron Gas (2DEG) shows excellent carrier mobility and current density.

[1] K. R. Bagnall, "Device-level thermal analysis of gan-based electronics," Ph.D. dissertation, Massachusetts Institute of Technology, 2013.

Thermal Challenges

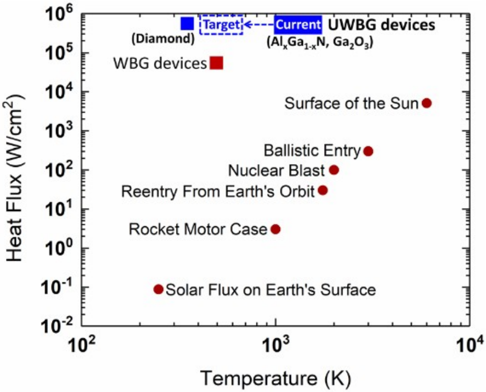

Figure 3: The heat flux challenge of WBG and UWBG power electronic devices (persuming operation at $\sim 10\,\mathrm{W/mm}$).[2]

[2] S. Choi, S. Graham, S. Chowdhury, *et al.*, "A perspective on the electro-thermal co-design of ultra-wide bandgap lateral devices," *Applied Physics Letters*, vol. 119, no. 17, p. 170 501, 2021.

Thermal Issues in GaN HEMTs

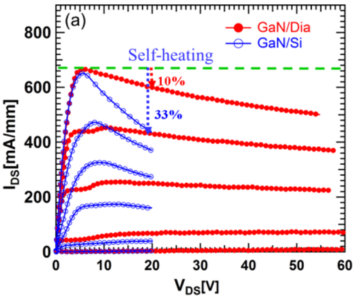

Figure 4: $I_{\mathrm{DS}} - V_{\mathrm{DS}}$ of GaN/Dia and GaN/Si HEMTs [3].

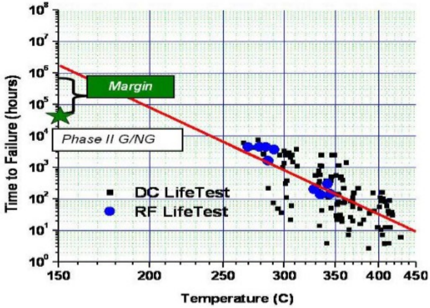

Figure 5: Mean time to failure (MTTF) for TriQuint GaN PAs [4].

The significant overheating within the devices largely degrades the electrical performance and shortens the device lifetime.

[3] K. Ranjan, S. Arulkumaran, G. Ng, *et al.*, “Investigation of self-heating effect on dc and rf performances in algan/gan hemts on cvd-diamond,” *IEEE Journal of the Electron Devices Society*, vol. 7, pp. 1264–1269, 2019.

[4] M. Rosker, C. Bozada, H. Dietrich, *et al.*, “The darpa wide band gap semiconductors for rf applications (wbgs-rf) program: Phase ii results,” *CS ManTech*, vol. 1, pp. 1–4, 2009.

Bias Dependence of Self-Heating

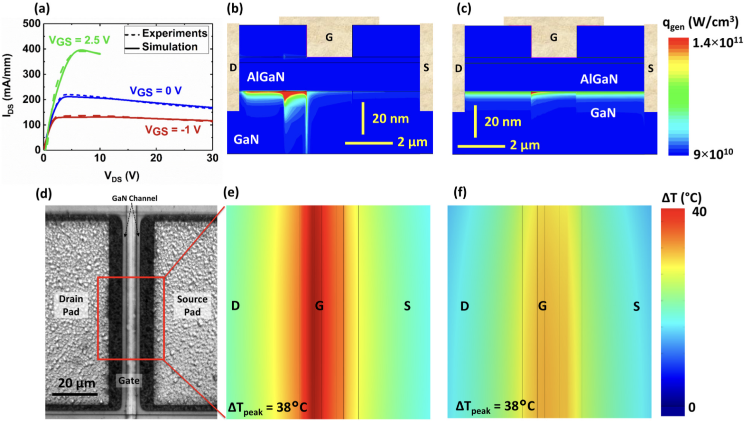

Figure 6: Bias dependent results for channel conditions with $V_{GS} = -1\,\text{V}$ and $V_{GS} = 2.5\,\text{V}$, respectively[5], $P_{diss} = 250\,\text{mW}$.

[5] B. Chatterjee, C. Dundar, T. E. Beechem, *et al.*, "Nanoscale electro-thermal interactions in algan/gan high electron mobility transistors," *Journal of Applied Physics*, vol. 127, no. 4, p. 044 502, 2020.

Electrothermal Simulation

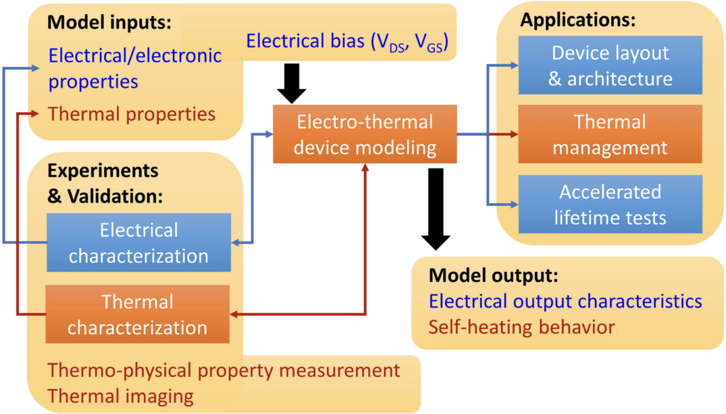

Figure 7: Flow diagram of the device-levelelectro-thermal co-design process[6].

[6] S. Choi, S. Graham, S. Chowdhury, *et al.*, "A perspective on the electro-thermal co-design of ultra-wide bandgap lateral devices," *Applied Physics Letters*, vol. 119, no. 17, p. 170 501, 2021.

Multiscale Electrothermal Transport

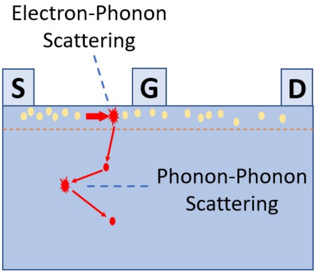

(a) Schematic of energy carriers interaction in GaN HEMTs.

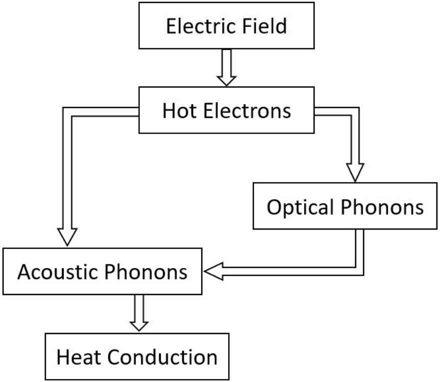

(b) Most likely path between energy carrying particles in a semiconductor device.

Figure 8: Schematic of energy transport in GaN HEMTs.

Macroscopic Simulation

Conservation equation + Constitutive model

Electron Part

Poisson equation + Electron continuity equation + DDM model

$$\nabla \cdot (\varepsilon \nabla \psi) = -q\,(p - n + N_D - N_A)$$

$$-\frac{1}{q} \nabla \cdot \mathbf{J_n} = G - R$$

$$\frac{\mathbf{J}_n}{q} = D_n \nabla n - n \mu_n \nabla \psi$$

Thermal Part

Energy equation + Fourier model

$$-\nabla \cdot (k \nabla T) = \frac{1}{q} \vec{J}_n \cdot \nabla E_C + \frac{1}{q} \vec{J}_p \cdot \nabla E_V$$

3D Device Simulation

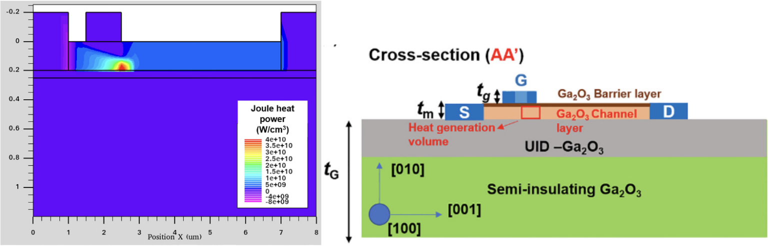

(a) (b)

Figure 9: TCAD + FEM simulation process[7]. Import 2D heat generation profile calculated by electrical simulations to 3D thermal FEM models.

[7] C. Yuan, Y. Zhang, R. Montgomery, *et al.*, "Modeling and analysis for thermal management in gallium oxide field-effect transistors," *Journal of Applied Physics*, vol. 127, no. 15, p. 154 502, 2020.

Parametric Study

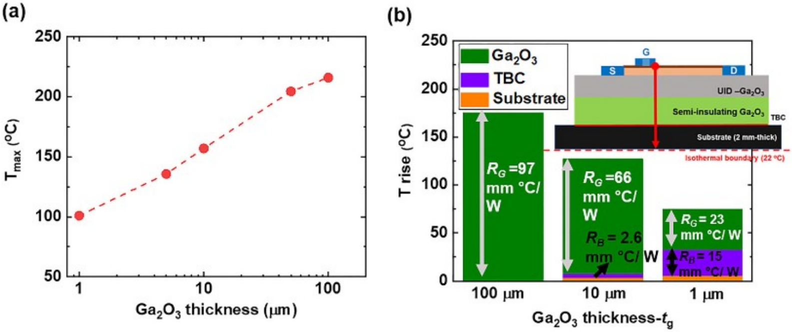

Figure 10: (a) The dependence of channel maximum temperature on Ga_2O_3 thickness (b) Modeled temperature rise for the Ga_2O_3-TBC-substrate structure.

Combined with Phonon Monte Carlo Simulation

Phonon BTE domain: $7 \times 3\mu m^2$, heat source obtained from TCAD simulation, thermal boundary conditions obtained from Fourier simulation[8].

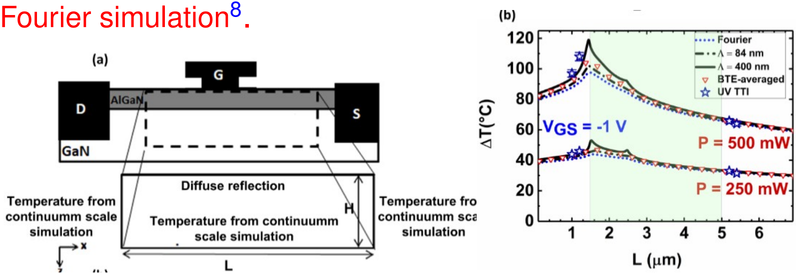

(a) (b)

Figure 11: (a) Schematic of the thermal domain modeled to observe the ballistic-diffusive thermal transport and relevant boundary conditions. (b) Comparison of temperature profiles obtained by continuum scale electrothermal simulation and BTE models.

---

[8] B. Chatterjee, C. Dundar, T. E. Beechem, *et al.*, "Nanoscale electro-thermal interactions in algan/gan high electron mobility transistors," *Journal of Applied Physics*, vol. 127, no. 4, p. 044 502, 2020.

Hydrodynamic Model

Boltzmann transport equation:

$$\frac{\partial f}{\partial t} + \frac{\mathbf{p}}{m} \cdot \nabla f + \mathbf{F} \cdot \frac{\partial f}{\partial \mathbf{p}} = \left(\frac{\partial f}{\partial t}\right)_{\mathrm{coll}}$$

$f(t, x, y, z, p_x, p_y, p_z)$ is a 7 dimensional function!

Moment method for BTE: Reduce the dimension from 7 to 4 by integration over momentum space and close the equations under some assumptions.

$$e.g. \quad n = \int f \mathrm{d}^3 p$$

Governing Equations

$$\nabla^2 V = -\frac{e}{\varepsilon_s}(N_D - n)$$

$$\frac{\partial n}{\partial t} + \nabla \cdot (n\vec{v}) = \left(\frac{\partial n}{\partial t}\right)_c$$

$$\frac{\partial \vec{p}}{\partial t} + \nabla \cdot (\vec{v}\vec{p}) = -en\vec{E} - \nabla (nk_B T_e) + \left(\frac{\partial \vec{p}}{\partial t}\right)_c$$

$$\frac{\partial W_e}{\partial t} + \nabla \cdot (\vec{v} W_e) = -en\vec{v} \cdot \vec{E} - \nabla \cdot (\vec{v} nk_B T_e)$$

$$-\nabla \cdot (-k_e \vec{\nabla} T_e) + \left(\frac{\partial W_e}{\partial t}\right)_c$$

$$\frac{\partial W_{LO}}{\partial t} = -\left(\frac{\partial W_e}{\partial t}\right)_c + \left(\frac{\partial W_{LO}}{\partial t}\right)_c$$

$$\frac{\partial W_a}{\partial t} = \nabla \cdot (k_a \nabla T_a) - \left(\frac{\partial W_{LO}}{\partial t}\right)_c$$

Collision Terms

Relaxation time approximation:

$$\left(\frac{\partial n}{\partial t}\right)_c = 0$$

$$\left(\frac{\partial \vec{p}}{\partial t}\right)_c = -\frac{\vec{p}}{\tau_m} = -\frac{m^* n \vec{v}}{\tau_m}$$

$$\left(\frac{\partial W_e}{\partial t}\right)_c = -\frac{w - w_0}{\tau_{e-LO}} = -n\frac{\frac{3}{2}k_B T_e + \frac{1}{2}m^* v^2 - \frac{3}{2}k_B T_{LO}}{\tau_{e-LO}}$$

$$\left(\frac{\partial W_{op}}{\partial t}\right)_c = -C_{LO}\frac{T_{op} - T_a}{\tau_{op-a}}$$

Closed Governing Equations

Variables to be solved: V, n, T_e, T_{LO}, T_A

$$\nabla^2 V = -\frac{e}{\varepsilon_s}(N_D - n), \vec{E} = -\nabla V$$

$$\frac{\partial n}{\partial t} - \nabla \cdot \left\{ n\mu\vec{E} + \frac{\mu}{e}\nabla(nk_B T_e) \right\} = 0$$

$$\frac{\partial T_e}{\partial t} + \nabla \cdot (\vec{v} T_e) = \frac{1}{3} T_e \nabla \cdot \vec{v} + \frac{2}{3nk_B}\nabla \cdot (k_e \nabla T_e)$$
$$+ \frac{m^* v^2}{3k_B}\left(\frac{2}{\tau_m} - \frac{1}{\tau_{e-LO}}\right) - \frac{T_e - T_{LO}}{\tau_{e-LO}}$$

$$C_{LO}\frac{\partial T_{LO}}{\partial t} = \frac{3}{2}nk_B\frac{T_e - T_{LO}}{\tau_{e-LO}} + \frac{nm^* v^2}{2\tau_{e-LO}} - C_{LO}\frac{T_{LO} - T_A}{\tau_{LO-A}}$$

$$C_A\frac{\partial T_A}{\partial t} = \nabla \cdot (k_A \nabla T_A) + C_{LO}\frac{T_{LO} - T_A}{\tau_{LO-A}}$$

Some Results

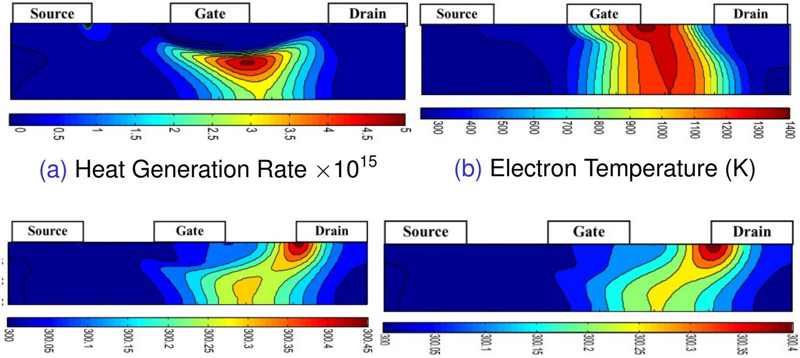

(a) Heat Generation Rate $\times 10^{15}$

(b) Electron Temperature (K)

(c) LO-phonon Temperature (K)

(d) Acoustic phonon Temperature (K)

Figure 12: Calculated thermal characteristics in GaN device[9].

[9] A. Fan, C. Tarau, R. Bonner, *et al.*, “2-d simulation of hot electron-phonon interactions in a submicron gallium nitride device using hydrodynamic transport approach,” in *Heat Transfer Summer Conference*, American Society of Mechanical Engineers, vol. 44786, 2012, pp. 685–693.

Electron Monte Carlo Simulation

$$\frac{\partial f(\bar{x},\bar{k},t)}{\partial t}+\frac{1}{\hbar}\nabla_{\bar{k}}\mathcal{E}(\bar{k})\nabla_{\bar{x}}f(\bar{x},\bar{k},t)+\frac{qE(\bar{x},t)}{\hbar}\nabla_{\bar{k}}f(\bar{x},\bar{k},t)=\left[\frac{\partial f}{\partial t}\right]_{\text{collision}}$$

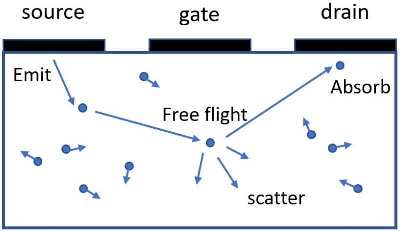

Figure 13: Schematic of electron monte carlo simulation.

The motion of an electron is described by two quantities, i.e. the position vector $\bar{x}$ and pseudo-wave vector $\bar{k}$.

$$\frac{d\bar{x}}{dt}=\frac{1}{\hbar}\nabla_{\bar{k}}\varepsilon(\bar{k}),\ \frac{d\bar{k}}{dt}\quad=\frac{q\bar{E}}{\hbar},\tau=-\frac{\ln(r_1)}{\Gamma}$$

Electron Monte Carlo Simulation[10]

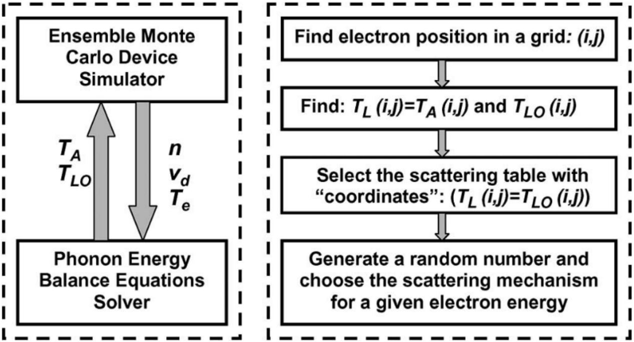

Figure 14: Exchange of variables between the electron system and phonon system.

The different systems are connected only by carrier scattering, the transfered information is only used in scattering rates!

[10] K. Raleva, D. Vasileska, S. M. Goodnick, *et al.*, "Modeling thermal effects in nanodevices," *IEEE Transactions on Electron Devices*, vol. 55, no. 6, pp. 1306–1316, 2008.

Phonon Temperature Bottleneck

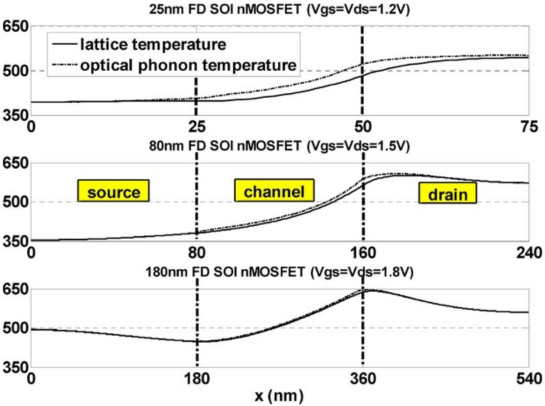

Figure 15: Averaged lattice and optical phonon temperature profiles in the channel direction.

The energy transfer between the optical and acoustic phonons is slow compared with the electron-optical phonon processes.

Hybrid Monte Carlo Simulation[11]

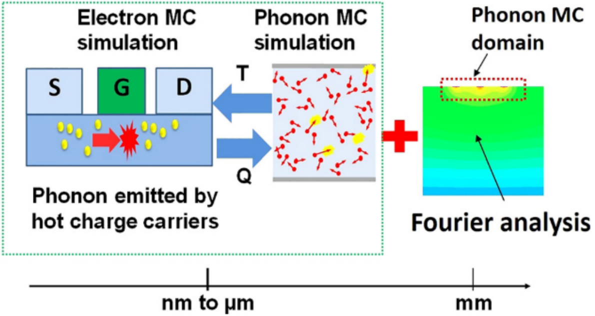

Figure 16: Scheme of multi-length scale electrothermal simulations of a GaN HEMT.

[11] Q. Hao, H. Zhao, and Y. Xiao, "A hybrid simulation technique for electrothermal studies of two-dimensional gan-on-sic high electron mobility transistors," *Journal of Applied Physics*, vol. 121, no. 20, p. 204 501, 2017.

Simulation Process

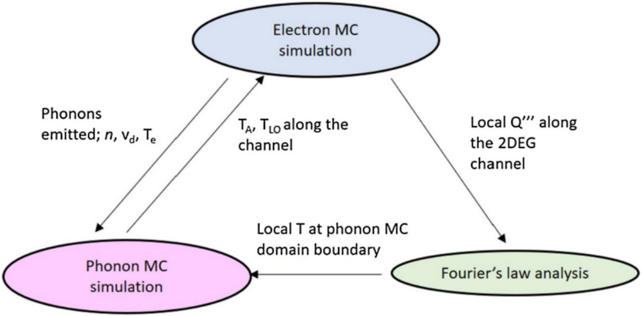

Figure 17: The feedbacks between electron MC simulations, phonon MC simulations, and Fourier's law analysis. The electron and phonon MC simulations are for the transistor region only, whereas the Fourier's law analysis is for the whole sub-mm chip[12].

[12] Q. Hao, H. Zhao, Y. Xiao, *et al.*, "Electrothermal studies of gan-based high electron mobility transistors with improved thermal designs," *International Journal of Heat and Mass Transfer*, vol. 116, pp. 496–506, 2018.

Schemaic of Simulated GaN HEMT

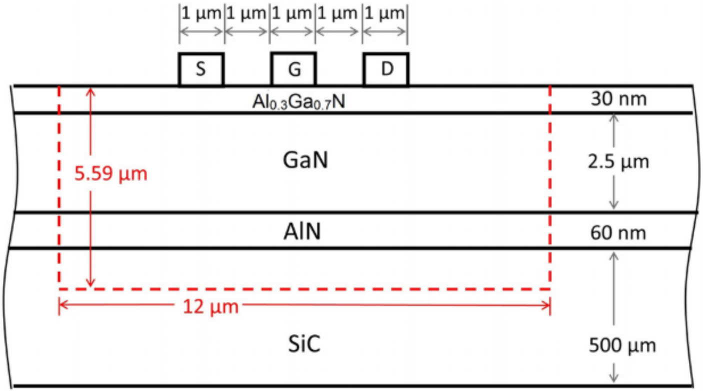

Figure 18: Schematic diagram of the cross section of the simulated GaN HEMT. The region enclosed by the dashed line is the domain for phonon MC simulations.

Comparison with Macroscopic Methods

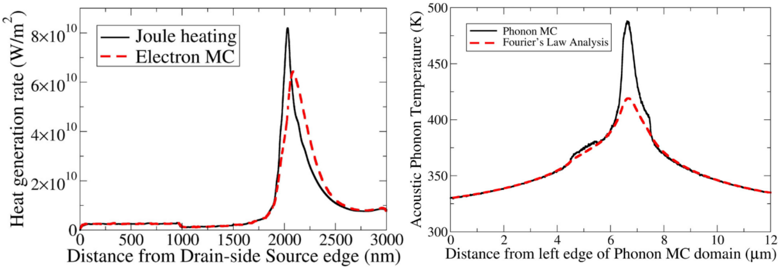

(a) Heat generation rate (b) Acoustic phonon temperature

Figure 19: Comparison of results at 2DEG between the hybrid simulation and macroscopic approaches.

Real 3D Multi-finger Simulation

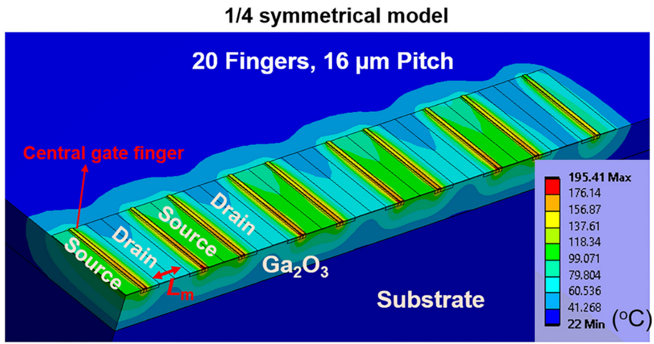

Figure 20: A 3D finite element model for multi-finger transistors[13].

In 3D thermal simulations of real devices (*e.g.* optimization of the epitaxial structure), FEM still plays a major role.

[13] C. Yuan, Y. Zhang, R. Montgomery, *et al.*, "Modeling and analysis for thermal management in gallium oxide field-effect transistors," *Journal of Applied Physics*, vol. 127, no. 15, p. 154 502, 2020.

Uncertainty in Real Devices

Table 1: Measurement of thermophysical properties of GaN HEMTs with different substrates.

Sample	Thermophysical property		
	k_{GaN} / $\text{Wm}^{-1}\text{K}^{-1}$	$k_{\text{GaN}}/\text{Wm}^{-1}\text{K}^{-1}$	TBR / $\text{m}^2\text{K}\cdot\text{GW}^{-1}$
Si-substrate	143.1 ± 6.5	114.8 ± 2.2	16.5 ± 4.1
SiC-substrate	182.5 ± 26.4	309.3 ± 12.0	8.4 ± 2.9

Difference between Models and Real Devices

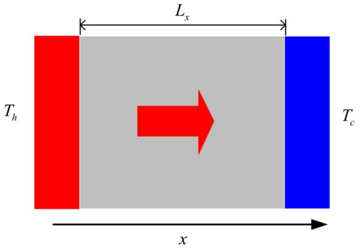

(a) Schematic of measurement of thermal conductivity of thin films.

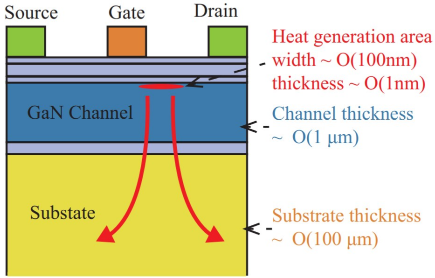

(b) Schematic of heat transport in GaN HEMTs.

The degeneration of k_{eff} is caused by the depression of phonon MFPs induced by phonon-boundary scattering, defects, interfaces, heating method, and heat source distribution, etc. will significantly affect k_{eff}!

Bias Dependence of Non-Fourier Heat Conduction in GaN HEMTs

Objective:

Reexamine the bias dependence of self-heating in GaN HEMTs by using TCAD and hybrid Monte Carlo-diffusion simulations.

Try developing thermal resistance model that can take the bias dependence and the influence of ballistic effects into account.

Device Structure[14]

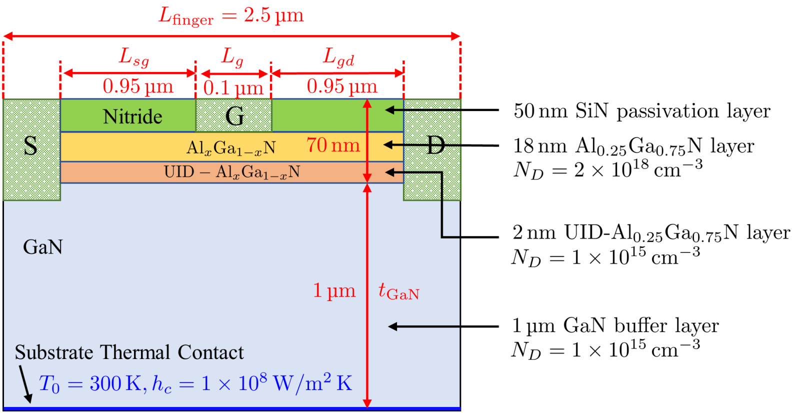

Figure 21: Schematic of GaN HEMT. The geometries are not drawn to scale.

[14] X. Chen, S. Boumaiza, and L. Wei, "Self-heating and equivalent channel temperature in short gate length gan hemts," *IEEE transactions on electron devices*, vol. 66, no. 9, pp. 3748–3755, 2019.

Output Characteristics

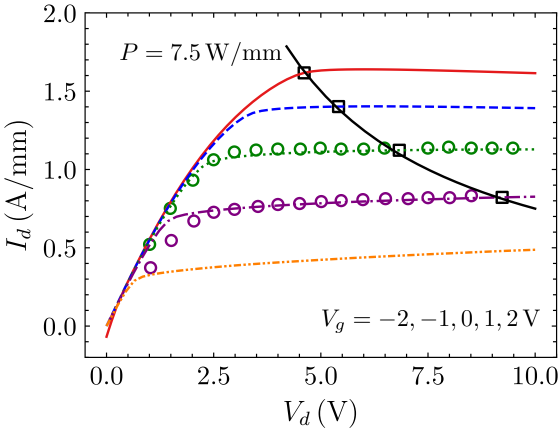

Figure 22: Output characteristics of the HEMT under V_g from $-2\,\mathrm{V}$ to $2\,\mathrm{V}$ with an interval of $1\,\mathrm{V}$.

Bias-Dependent Heat Generation

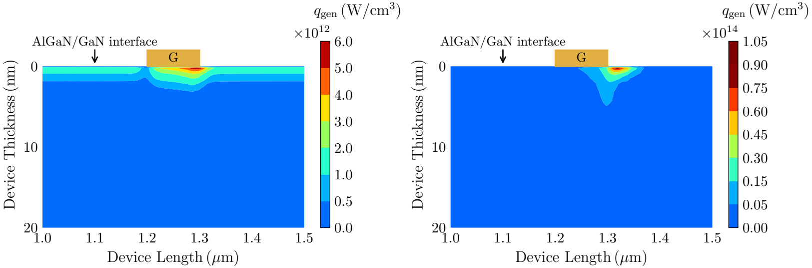

(a) $V_g = 2\,\text{V}$, $V_d = 4.5\,\text{V}$ (b) $V_g = -1\,\text{V}$, $V_d = 9.5\,\text{V}$

Figure 23: The total power dissipation level for the two bias conditions, $P = 7.5\,\text{W/mm}$.

GaN on SiC HEMT

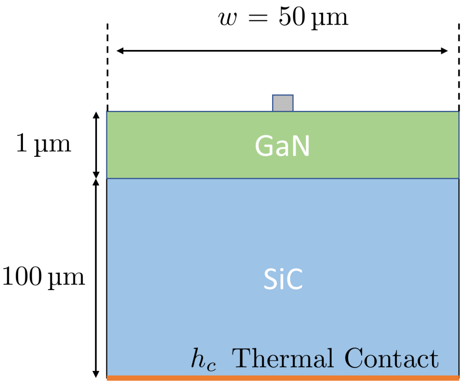

Figure 24: Expected simulated GaN on SiC HEMT.

TCAD calculated heat generation profile $\Rightarrow$ hybrid Monte Carlo-diffusion simulation

Keep Developing...

santashen refactor: 重构界面的实现 ... 141a6f4 4 minutes ago 8 commits

README	docs: add front cover	last month
docs	feat(All): release first version	6 months ago
examples	feat(All): release first version	6 months ago
shengmc	refactor: 重构界面的实现	4 minutes ago
README.md	docs: add front cover	last month
setup.py	refactor: by pass arccos calculation.	last month

README.md

shengmc

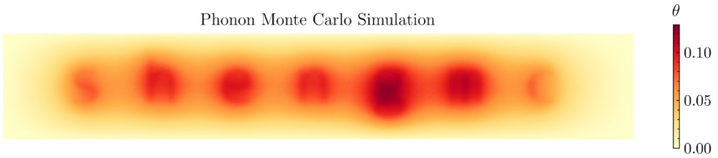

Thank You!